Deflections of pneumatic masts and columns

Jean-Christophe Thomas, Anh Le Van

Deflections of pneumatic masts and columns

J.-C. Thomas and A. Le Van

GeM (Institute for Research in Civil and Mechanical Engineering), Université de Nantes-École Centrale Nantes, Nantes Cedex 3, France

Like all structural elements, inflatable beams can be subjected to combined loads. This may be the case for inflatable masts or inflatable columns supporting floors. This study addresses inflatable beams subjected to combinations of compression and bending. Whereas the mechanics of inflatable beams subjected only to transverse loading is now well established, the study of inflatable beams subjected to combined loads has still received few investigation. Furthermore, whereas the effects of individual loads are superimposed when beams are made of conventional materials such as steel, the problem is more complex for inflatable beams since compressive forces counteract the effects of internal pressure and reduce the stiffness. This study presents new analytical formulas for inflatable beams subjected to bending and compressive loads. Buckling load and wrinkling limit load are also proposed, taking into account the internal pressure.

Introduction

Pneumatic structures are an important part of lightweight tensile structures. Flexible, lightweight, adaptable, they are easy to carry, easy to deploy and erect, easy to disassemble and easy to store. They can be designed for short events and also for much longer duration. They can be classified into different emblematic typologies: air-supported structures which are mono-membranes inflatable structures, air-inflated structures also named inflatables, which are generally composed of air beams or/and air cushions, and hybrid structures, which can be composed of both. All these typologies can be seen on the tensinet website (Tensinet, http://www.tensinet.com).

Air beams are the simplest inflatable structure to understand key steps of the behavior: deflection of the beam subjected to bending loading, wrinkling that occurs when a wrinkle appears somewhere in the membrane, collapse of the beam when the bent beam does not resist any more and buckling in the case of pure compression. Some previous studies have been conducted on these different important topics and allow predicting precisely the behavior of inflatable beams (Fichter, 1966; Le van & Wielgosz, 2005; Nguyen, Thomas, & Le Van, 2013a, 2015; Thomas & Bloch, 2016).

In the frame of the work of the Working Group 5 of CEN TC 250, which aims to write a Eurocode dedicated to membrane structures, it is important to precisely know the performance of the models used to design membrane structures. The rules of design should be obtained by reliability analysis for which estimations of the accuracy of the design is a current and important issue. In the case of air beams subjected to transverse loads, the analytical results have been compared with 3D simulation results and experiments. For example, the performance of these models have been estimated by

CONTACT J.-C. Thomas jean-christophe.thomas@univ-nantes.fr GeM (Institute for Research in Civil and Mechanical Engineering), University of Nantes-École Centrale Nantes, UMR CNRS 6183 2, rue de la Houssinière, BP 92208, 44322 Nantes Cedex 3, France

comparison with experimental results in the case of supported beams and used to conduct a reliability analysis of a pedestrian inflatable bridge (Thomas, Schoefs, Caprani, & Rocher, 2018).

Whereas the behavior of inflatable beams under bending load is well mastered, the case of combined loading has not been studied, in particular the case of the air beams subjected to both compression and bending loads. This case can occur if one seeks to build inflatable masts, for example to support urban lighting devices or monitoring devices, which can be heavy compared to the weight of the beams that support these devices (Figure 1(a)). Another possibility, which is rather in the field of the prospective today, but could quite quickly appear, concerns columns supporting floors (Figure 1(b)). The difference between these two configurations concerns the extreme cross-section of the beam that can rotate in the case of a mast, or remain horizontal on the case of a column supporting a floor.

When the beams are made of conventional materials like steel, aluminum or concrete for example, it is usual to superimpose the effects of the separated actions. However, the case of air beams is specific because there stiffness come from the pretension due to the pressure inside the beam. This pressure acts on the ends of the beams and gives a normal load that is transmitted in the membrane along the beam. The pretension leads then to a reserve of positive stresses in the axial direction. Compression forces counteract this pretension specific to air beams and it is then necessary to conduct a study to properly account for the combination of the longitudinal effect of the internal pressure and the compression axial load that is superimposed.

To solve this problem, in a first step, we propose to consider again the important points of the previous studies and show how to adapt the results of the bending formulas to take into account the compressive stress. We will then make comparisons with the results of a 3D homemade code named SAFE in the case of the inflatable mast. The code SAFE is dedicated to membrane structures, it is based on the total Lagrangian formulation and the resulting nonlinear equilibrium equation is solved by means of the iterative Newton scheme. With regards to material, the membrane material can be orthotropic to represent the behavior of coated fabrics which are usually used in inflatable structures.

The behavior of coated fabric membrane structures is complex. The results of biaxial tensile experiments highlight the non-linear behavior of the material (Bridgens, Gosling, Jou, & Hsu, 2012; Galliot & Luchsinger, 2009; Quaglini, Corazza, & Pogi, 2008). Different models have been proposed to represent the behavior of coated fabrics. For example (Bridgens & Gosling, 2004) proposed a model based on response surfaces, (Galliot & Luchsinger, 2009) proposed an approach based on a linear elastic orthotropic model with constants varying according to the loading ratio between the warp and the weft, and more recently, Motevalli, Uhlemann, Stranghöner, and Balzani (2019) has proposed an approach based on hyperelastic orthotropic energy functions. These models are often complicated to implement in computer codes and, for the moment, the common practice is to use linear elastic constitutive laws from an engineering point of view.

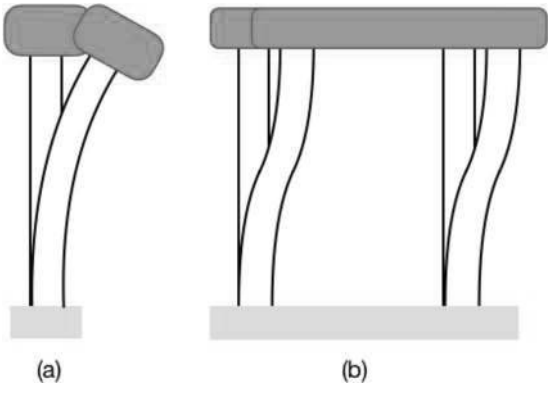

Figure 1. Inflatable mast (left) and column (right).

In our study, non-linearities are taken into account by using the total Lagrangian formulation. The assumption used for the material is an orthotropic linear elastic constitutive law and the non-linear behavior of the structure is addressed from the angle of geometric non-linearities. This model is used to write analytical formulae for inflatable beams and it is also the approach used in the 3D code SAFE that we use as a reference in the laboratory. These analytical models and the results of the numerical computations have proved very satisfactory in previous works on inflatable structures, and in particular with comparisons with experiments, for example for the inflation of pneumatic beams (Nguyen, Thomas, & Le Van, 2013b) or for the study of deflections and vibrations of inflatable beams (Thomas, Le Van, Aduriz, & Jiang, 2005).

In a second step, we will revisit the theory to present more rigorous formulas in order to improve the model. Finally, we will propose new formulas for the different cases proposed: inflatable mast and inflatable column. The buckling forces are also calculated, giving the upper bounds for the compressive loads.

Behavior of air beams

The natural state and notations

As explained above, the membrane is assumed to follow a linear orthotropic elastic constitutive law, within the framework of a total Lagrangian approach to represent the behavior of a coated fabric usually used to built such structures. Here, the fabric will be assumed to be oriented so that one of the main directions of the fabric, weft or warp, is parallel to the axis of the beam. Also, the membrane modeling the fabric has one of the orthotropic directions aligned with the beam axis. At any point on the membrane, it is therefore possible to define a local basis with the unit vectors $\overrightarrow{e_\ell}$ aligned with the longitudinal direction, $\overrightarrow{e_t}$ locally tangential to the fabric and orthogonal to $\overrightarrow{e_\ell}$, and $\overrightarrow{e_n}$ completing the direct basis and being locally normal to the membrane (see Figure 2). On this figure, the mesh represents the beam in the natural state, when the beam is not pressurized. The own weight of the membrane is neglected, so that the natural state is a cylinder. Due to symmetries, only one half of the beam is represented.

The bending movement of the beam is defined in the global coordinate system (x, y, z). We will only consider movements parallel to the (x, y) plane.

Key steps of the behavior of pneumatic beams

To fully understand the different states, let us look at the numerical results for a simply supported beam. Figures 3 and 4 show the specific stages of the beam's behavior. The red mesh corresponds to the natural state, and the grey mesh corresponds to the state of the

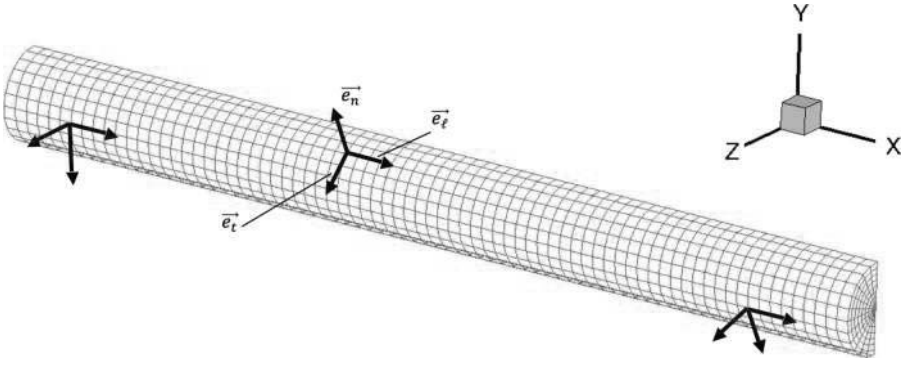

Figure 2. Local orthotropy basis.

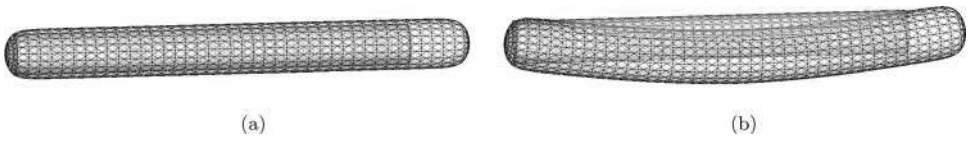

Figure 3. Inflation and bending of an inflatable beam. (a) First step: inflation. (b) Second step: bending.

pressurized and possibly loaded beam. Figure 3(a) represents the pressurization step which is an important step. At the end of this step the beam goes from the natural state to the initial state. This step is important for the rest of the study, as it defines the initial geometry, including the radius and the length. It also makes it possible to define the pre-tension stresses and the stiffness of the structure. The characteristic quantities will be denoted with a symbol ø when they are relative to the natural state, and without any particular sign when relative to the initial state. Thus, $R_{\emptyset}$ and $L_{\emptyset}$ are the radius and length of the beam in the natural state, while R and L correspond to these same dimensions in the initial state.

Figure 3(b) corresponds to the deflected state. Under transverse loading, the beam moves from the initial state to the actual state. Previous studies have shown that as long as a wrinkle does not appear, the relationship between deflection and loading can be considered linear (Nguyen et al., 2015; Thomas & Bloch, 2016). The load which should not be exceeded to avoid the onset of the wrinkle is called the wrinkling load. For conventional materials like aluminum, steel, concrete or wood, the material strength study is conducted between the initial and actual state and there exists no natural state. For inflatable beams, the pre-tensioning step is important and the transition from the natural to the initial state must also be considered.

The above mentioned loading level not to be exceeded to remain in the linear domain corresponds to the beginning of plasticity in the cases of conventional materials. The case of inflatable beams is specific and different. The first phase of linear behavior ends as soon as a wrinkle appears at the upper surface of the beam in the case of the supported beam. It is also important to note that the appearance of the wrinkle does not imply that the beam collapses. There still exists a reserve of stiffness. Increasing the load beyond the wrinkling load leads to a propagation of the wrinkle around the section (Figure 4(a)) and the collapse occurs when the wrinkle reaches the middle of the beam section (Figure 4(b)). This property had been theoretically and experimentally verified (Thomas & Bloch, 2016).

A parallel can be drawn between the plasticity loads in the case of conventional materials and the collapse loads of inflatable beams.

Note that there exists another interesting specificity of inflatables: when unloaded, inflatable beams come back to their initial state. It means that, if creep effects are neglected, the behavior can be considered as reversible. Reversible collapse might not be an appropriate terminology, but it is a physical reality in the case of inflatable beams.

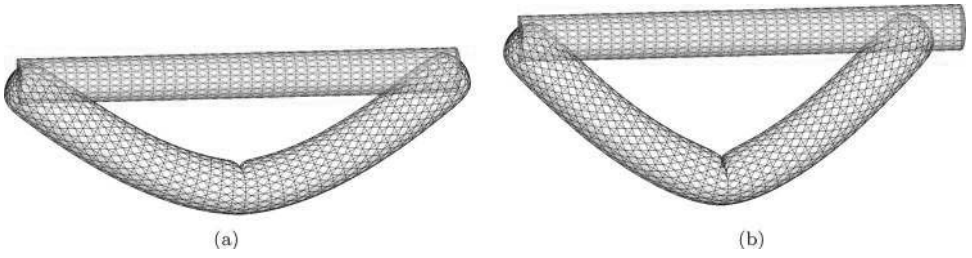

Figure 4. Inflated bended beam: propagation of wrinkle and collapse. (a) Wrinkle in the cross section. (b) Collapse of the beam.

Stresses in the membrane

To understand the behavior of inflatable beams, it is necessary to detail with precision the distribution of longitudinal stresses in the various cases of loading. Figure 5(a) shows the distribution of stresses when no wrinkle appears in the membrane. The longitudinal stresses due to the inflation (in grey) are superimposed with the longitudinal stresses due to the bending (in black). This leads to the final distribution (in blue). In the case shown, all the longitudinal stresses remain positive. Figure 5(b) presents the distribution of the stresses when a wrinkle appears in the membrane. This happens when one of the principal stress of the beam vanishes, as located by the red circle.

This allows to define a criterion: the wrinkling load is attained when the longitudinal stress vanishes in a point of the membrane. For example, in the case of a cantilever inflatable beam, it is possible to calculate the wrinkling load in terms of the pressure p and the geometric parameters:

$$F_W = \frac{p\pi R^3}{2L}. \tag{1}$$

Note that this result does not depend on the material coefficients (i.e. the elasticity moduli). They only affect the length and the radius in the initial state which are calculated from the length and the radius in the natural state. For moderate pressures, the radius and length are linear functions of the pressure. These following formulas can easily be obtained:

$$R = R_{\emptyset}\left(1 + \frac{pR_{\emptyset}}{2{}^{\emptyset}E_t}(2 - {}^{\emptyset}\nu_{t\ell})\right) \quad \text{and} \quad L = L_{\emptyset}\left(1 + \frac{pR_{\emptyset}}{2{}^{\emptyset}E_{\ell}}(1 - 2{}^{\emptyset}\nu_{\ell t}\right), \tag{2}$$

where ${}^{\emptyset}E_{\ell}$ and ${}^{\emptyset}E_t$ are the elasticity moduli in the longitudinal and transverse directions, ${}^{\emptyset}\nu_{t\ell}$ is a Poisson's coefficient.

Deflection of an uncompressed air beam

The details of the equations used in this paragraph can be found in Le van and Wielgosz (2005) and Nguyen et al. (2013a, 2015). These equations were obtained by applying the principle of virtual powers in large deformations in order to correctly take into account the effect of pressure on the side walls, using the total Lagrangian formulation. Since inflatable beams are very thin-walled beams, they are sensitive to shear. This is why it is necessary to use Timoshenko's kinematics: the cross-section of the beam remains plane after deformation while it does not remain perpendicular to the neutral line of the beam.

The air-beams made of coated fabrics are modeled in this study by orthotropic linear elastic membranes. The constitutive laws used are $\Sigma_{xx} = \Sigma^0_{xx} + E_{\ell}E_{xx}$ for the normal stress, and

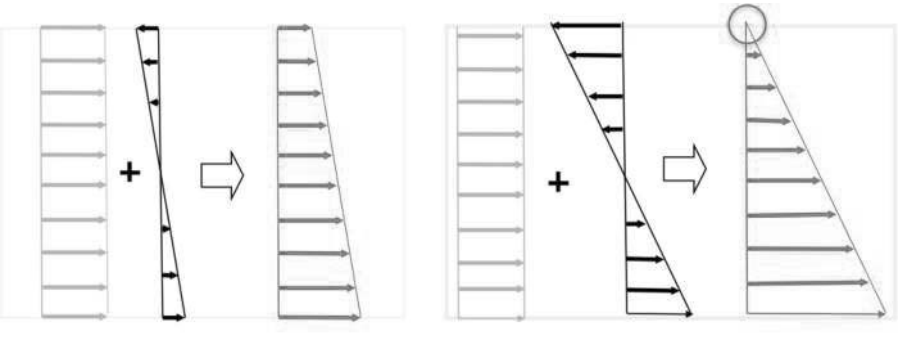

Figure 5. Distribution of the longitudinal stresses in the membrane. (a) Inflation and bending. (b) Onset of a wrinkle.

$\Sigma_{xy} = \Sigma^0_{xy} + G_{\ell t}E_{xy}$. Here, Σ^0_{xx} is the initial normal stress, and Σ_{xx} is the actual normal stress. The same distinction applies to the shear stress between Σ^0_{xy} and Σ_{xy}. E_ℓ is the Young modulus in the longitudinal direction, and $G_{\ell t}$ is the shear modulus.

It was shown in Nguyen et al. (2013a, 2015) that the elastic moduli E_ℓ and $G_{\ell t}$ defined from the initial configuration differ from the moduli ${}^{\emptyset}E_\ell$ and ${}^{\emptyset}G_{\ell t}$ based on the natural configuration by the following relationships (Equation (3)), involving the coefficients that characterize the geometry changes due to the pressurization phase. Thus, $k_x = L/L_\emptyset$ is related to the change in the beam length, and $k_\theta = R/R_\emptyset$ is related to the change in the radius, i.e. in the tube circumference.

$$\frac{E_\ell}{{}^{\emptyset}E_\ell} = \frac{k_x^3}{k_\theta} \quad \text{and} \quad \frac{G_{\ell t}}{{}^{\emptyset}G_{\ell t}} = k_x k_\theta. \tag{3}$$

Finally, the non-linear equations obtained are linearized in order to obtain the following system of linear equations (Equations (4) to (9)), including equilibrium equations and boundary conditions.

The configuration chosen is presented in Figure 6. The grey beam on the figure is subjected to loads applied at its ends that can be represented by forces in the *xy*-plane and torques orthogonal to this plane. For the strength of materials point of view, the entire study is reduced to the neutral line, in black on the figure. Thus, the axial forces F_{x1} and F_{x2}, the transverse forces F_{y1} and F_{y2}, and the torques Γ_1 and Γ_2 are theoretically applied at the ends of the line. The deformation of the beam is represented by its cross-section rotation $\theta(x)$ and the deflection $v(x)$ in the *xy*-plane.

The linearized equations are:

$$-\frac{\mathrm{d}N(x)}{\mathrm{d}x} = 0 \tag{4}$$

$$-(N + kG_{\ell t}S)\frac{\mathrm{d}^2 v(x)}{\mathrm{d}x^2} + (P + kG_{\ell t}S)\frac{\mathrm{d}\theta(x)}{\mathrm{d}x} = 0 \tag{5}$$

$$\left(E_\ell I + \frac{NI}{S}\right)\frac{\mathrm{d}^2\theta(x)}{\mathrm{d}x^2} + (P + kG_{\ell t}S)\left(\frac{\mathrm{d}v(x)}{\mathrm{d}x} - \theta\right) = 0. \tag{6}$$

Here, N is the normal force, S is the area of the cross-section, $P = p\pi R^2$ where p is the internal pressure, and I is the second moment of area. Note that P is equal to the force induced by the internal pressure on the circular end of the beam. Coefficient k is a weighting factor to account for the fact that shear stresses are not uniform in the section. k is 0.5 for thin-walled circular cross-sections.

The boundary conditions are:

$$N(0) - P = -F_{x1} \quad N(L) - P = F_{x2} \tag{7}$$

$$(N(0) + kG_{\ell t}S)\frac{\mathrm{d}v}{\mathrm{d}x}(0) - (P + kG_{\ell t}S)\theta(0) = -F_{y1}$$

$$(N^0(L) + kG_{\ell t}S)\frac{\mathrm{d}v}{\mathrm{d}x}(L) - (P + kG_{\ell t}S)\theta(L) = F_{y2} \tag{8}$$

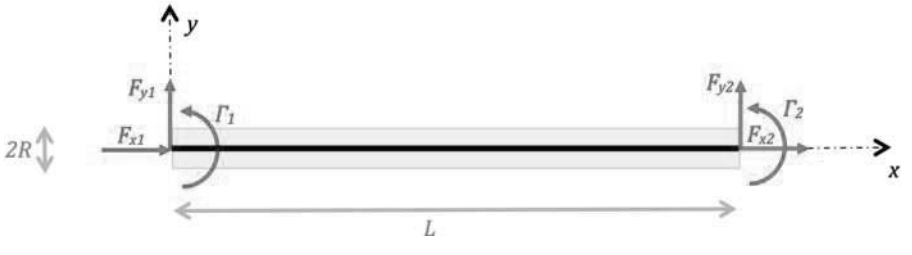

Figure 6. Forces and torques applied on an air-beam.

and

$$\left(E_\ell I + \frac{NI}{S}\right)\frac{\mathrm{d}\theta}{\mathrm{d}x}(0) = -\Gamma_1 \quad \left(E_\ell I + \frac{NI}{S}\right)\frac{\mathrm{d}\theta}{\mathrm{d}x}(L) = \Gamma_2. \tag{9}$$

Equation (4) shows that the normal load is uniform, $N(x) = cste$. In the case studied in this section, $F_{x1} = F_{x2} = 0$, then Equation (7) gives

$$N(x) = P. \tag{10}$$

This equality allows to notably simplify Equation (5) by collecting the term $P + kG_{\ell t}S$ and ones finally finds $(P + kG_{\ell t}S)(\mathrm{d}^2v/\mathrm{d}x^2 - \mathrm{d}\theta/\mathrm{d}x) = 0$. Then using the boundary condition (8) yields

$$\frac{\mathrm{d}v(x)}{\mathrm{d}x} = \theta(x) + \frac{F_{y2}}{P + kG_{\ell t}S}. \tag{11}$$

The last equation clearly shows the influence of the shear: the cross-section of the beam does not remain orthogonal to the neutral fiber since $\frac{dv}{dx} \neq \theta$. Let us consider now a cantilever air-beam, subjected to a transverse force $F_{y2} = F$ and a torque $\Gamma_2 = \Gamma$. Equation (6) gives $(EI + NI/S)(\mathrm{d}^2\theta/\mathrm{d}x^2) = -F$. Taking into account the boundary conditions (9) and $\theta(0) = 0$ and $v(0) = 0$ leads to:

$$\theta(x) = \frac{1}{E_\ell I + \frac{PI}{S}}\left(F\left(Lx - \frac{x^2}{2}\right) + \Gamma x\right), \tag{12}$$

$$v(x) = \frac{1}{E_\ell I + \frac{PI}{S}}\left(F\left(L\frac{x^2}{2} - \frac{x^3}{6}\right) + \frac{\Gamma x^2}{2}\right) + \frac{Fx}{P + kG_{\ell t}S}. \tag{13}$$

This result shows clearly the influence of the internal pressure on both stiffness: it increases the bending stiffness $E_\ell I$ and the shear stiffness $kG_{\ell t}S$. This is in line with intuition: the higher the internal pressure, the more rigid the beam becomes.

It is then possible to determine the stiffness of inflatable beams in both mast and column configurations, neglecting here the compression of the beam. The case of the column supporting an upper floor can be modeled, noting that the straight section linked to the floor does not rotate. The connection at this end can be modeled by a sliding clamp as shown in Figure 7.

Finally, the mast is modeled as a classic cantilever beam, and the column as a clamped beam at one end, and connected at the other end by a sliding clamp.

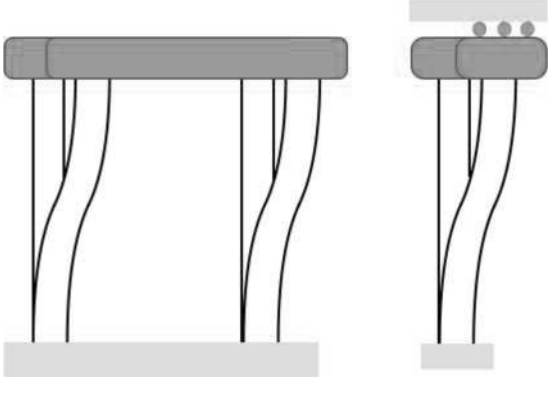

Figure 7. Clamp and sliding clamp for the column.

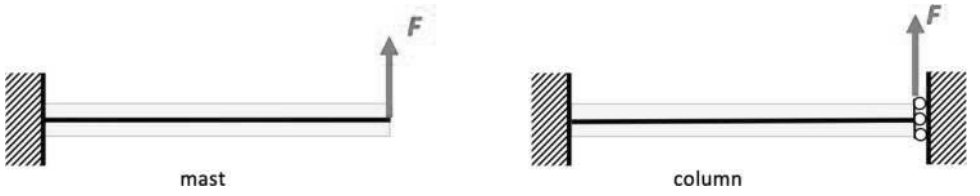

Figure 8. Uncompressed mast and column beam models.

The stiffness of the beams in both configurations are obtained by applying a transverse force F bending the beams (see Figure 8), and calculating their deflections $v_1(L)$ for the configuration 1 representing the mast and $v_2(L)$ for the configuration 2 corresponding to the column.

The formula (13) allows to obtain the results almost directly. For the first configuration, just put $\Gamma = 0$ in Equation (13), and for the second configuration, the corresponding moment Γ can be calculated using $\theta(L) = 0$ in the Equation (12), which gives $\Gamma = -FL/2$. It then remains to replace Γ by its value in (13).

The results are:

$$v_1(x) = \frac{F(L\frac{x^2}{2} - \frac{x^3}{6})}{E_\ell I + \frac{PI}{S}} + \frac{Fx}{P + kG_{\ell t}S} \quad \Rightarrow \quad v_1(L) = \frac{FL^3}{3(E_\ell I + \frac{PI}{S})} + \frac{F\ell}{P + kG_{\ell t}S} \tag{14}$$

and

$$v_2(x) = \frac{F(L\frac{x^2}{4} - \frac{x^3}{6})}{E_\ell I + \frac{PI}{S}} + \frac{Fx}{P + kG_{\ell t}S} \quad \Rightarrow \quad v_2(L) = \frac{FL^3}{12(E_\ell I + \frac{PI}{S})} + \frac{F\ell}{P + kG_{\ell t}S}. \tag{15}$$

Behavior of compressed air beams

Including the compression in the air-beam model

The equations in the previous sections do not take into account the compressive force that can be applied to the beam. The next step is to work on the following models: the cantilever beam subjected to an additional compressive force Q, which corresponds to a model of the compressed mast, and the beam clamped at one end, connected by a sliding clamp at its other end and compressed, which corresponds to the column carrying a load. In the case of the column, it should be noted that the sliding clamp connection is not a connection with the base, as in the uncompressed case. It is necessary to add an additional component that is in translation with respect to the base to be able to transmit the compression force and for the beam to contract freely in length. The models and boundary conditions are shown in Figure 9.

A new initial state

In both cases, it is necessary to redefine the initial state, which no longer corresponds to the pressurized beam but to the pressurized and compressed beam. This should logically reduce the initial length compared to the uncompressed beam and increase its radius. These variations will be computed assuming small deformations during this step. The constitutive law is then:

$$\begin{Bmatrix} \epsilon_{\ell\ell} \\ \epsilon_{tt} \\ \epsilon_{\ell t} \end{Bmatrix} = \begin{bmatrix} \frac{1}{\nu E_\ell} & -\frac{\nu_{\nu_{t\ell}}}{\nu E_t} & 0 \\ -\frac{\nu_{\nu_{\ell t}}}{\nu E_\ell} & \frac{1}{\nu E_t} & 0 \\ 0 & 0 & \frac{1}{\nu G_{\ell t}} \end{bmatrix} \begin{Bmatrix} \sigma_{\ell\ell} \\ \sigma_{tt} \\ \sigma_{\ell t} \end{Bmatrix} \tag{16}$$

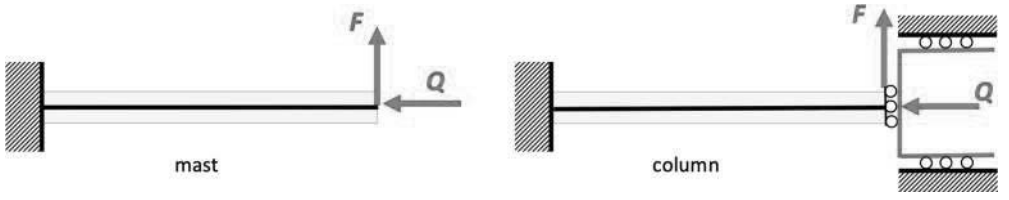

Figure 9. Compressed mast and column beam models.

The small deformation hypothesis allows the use of Cauchy stresses $\sigma_{\ell\ell}$, σ_{tt} and $\sigma_{\ell t}$, and the strains $\epsilon_{\ell\ell}$, ϵ_{tt} and $\epsilon_{\ell t}$.

The pressure p and force Q are related to the stresses by:

$$\sigma_{\ell\ell} = p\frac{R_\emptyset}{2} - \frac{Q}{2\pi R_\emptyset} \quad \text{and} \quad \sigma_{tt} = pR_\emptyset. \tag{17}$$

Using $\epsilon_{\ell\ell} = (L - L_\emptyset)/L_\emptyset$ and $\epsilon_{tt} = (R - R_\emptyset)/R_\emptyset$ leads to:

$$R = R_\emptyset\left(1 + \frac{pR_\emptyset}{2^\emptyset E_t}\left(2 - {}^\emptyset\nu_{t\ell}\left(1 - \frac{Q}{P}\right)\right)\right) \tag{18}$$

and

$$L = L_\emptyset\left(1 + \frac{pR_\emptyset}{2^\emptyset E_\ell}\left(1 - 2^\emptyset\nu_{\ell t} - \frac{Q}{P}\right)\right). \tag{19}$$

In Equations (18) and (19), the increase in Q leads to a decrease in the length of the beam, and an increase in its radius. Logically, if $Q = 0$, the expressions reduce to equation (2) for the pressurized and uncompressed beam.

Solution obtained by adapting the inflatable beam solution

The compression counteracts the background effect $P = p\pi R^2$ applied to the ends of the beam. The normal effort P is replaced by $P–Q$. It seems logical then to take into account the influence of compression by replacing P by $P–Q$ in the solutions (14) and (15). This immediately provides the solution for the mast-type beam $v_3(x)$ and the solution for the column-type beam $v_4(x)$:

$$v_3(x) = \frac{F(L\frac{x^2}{2} - \frac{x^3}{6})}{E_\ell I + \frac{(P-Q)I}{S}} + \frac{Fx}{P - Q + kG_{\ell t}S} \quad \text{so} \quad v_3(L) = \frac{FL^3}{3(E_\ell I + \frac{(P-Q)I}{S})} + \frac{F\ell}{P - Q + kG_{\ell t}S} \tag{20}$$

and

$$v_4(x) = \frac{F(L\frac{x^2}{4} - \frac{x^3}{6})}{E_\ell I + \frac{(P-Q)I}{S}} + \frac{Fx}{P - Q + kG_{\ell t}S} \quad \text{so} \quad v_4(L) = \frac{FL^3}{12(E_\ell I + \frac{(P-Q)I}{S})} + \frac{F\ell}{P - Q + kG_{\ell t}S}. \tag{21}$$

These expressions have been obtained without proof and it is necessary to justify their validation before going any further. In the following paragraph, the analytical solution corresponding to the mast $v_3(x)$ will be compared with those of the 3*D* code SAFE.

Comparison with the numerical 3D results

To assess the accuracy of the previous model, we propose to compare the results in the simplest case: the inflatable mast. The dimensions of the selected beam are given in Table 1. The ratio of the transverse dimension to the longitudinal dimension is 5. The longitudinal and transverse elastic moduli are

Table 1. Elasticity material coefficients and geometrical parameters.

Parameter in the natural state	Symbol	Value
Length	$L_{\emptyset}$	2.5 m
Radius	$R_{\emptyset}$	0.125
Longitudinal elasticity modulus	${}^{\emptyset}E_{\ell}$	210 kN/m
Transverse elasticity modulus	${}^{\emptyset}E_{t}$	210 kN/m
Shear elasticity modulus	${}^{\emptyset}G_{\ell t}$	50 kN/m
Poisson's coefficient	${}^{\emptyset}\nu_{\ell t}$	0.2

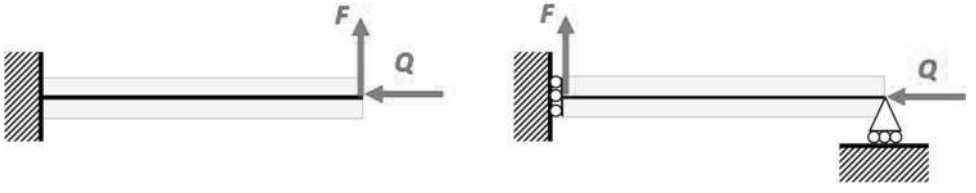

Figure 10. Boudary conditions for the 3D computations of the compressed bended beam.

taken equal, assuming a balanced fabric. The chosen elastic moduli have classical orders of magnitude for coated fabrics, whose shear modulus is much lower than the longitudinal and transverse elastic moduli.

The numerical simulations are performed with the code SAFE. The configuration used is the one on the right of the Figure 10 for practical reasons. It is a beam linked to the support by a sliding clamp at one end and a sliding support at its other end where it is subjected to compressive load. From the mechanical point of view, its behavior is completely identical to that of the left configuration.

Figure 11 shows the results of the 3D code for two different compression loads. The pressure is the same in both cases. The three transverse loads applied are of the same order of magnitude for both beams: $F = 60$ N, 156 N and 267 N for $Q = 100$ N, and $F = 61$ N, 169 N and 248 N for $Q = 300$ N. As these loads are very close for each calculation series, it can be deduced that the compression softens the beam. There is therefore a loss of rigidity. For the $Q = 300$ N case, note that the wrinkling load has been exceeded and a wrinkle has appeared, as shown by the red circle. This means that this result does not apply in this study since it is assumed that there are no wrinkle and that the cross-section of the beam remains circular.

Figure 12 shows the results of the 3*D* computations and the results of the analytical solution $v_3(x)$. It can be seen that for quite low compressive loads ($Q = 100$ N), v_3 gives correct results, but that as soon as the compressive load increases ($Q = 300$ N), the difference between the numerical result and the analytical result is significant, e.g. 43% for the example chosen for the highest transverse load. The model used here is therefore not satisfactory except for small compression.

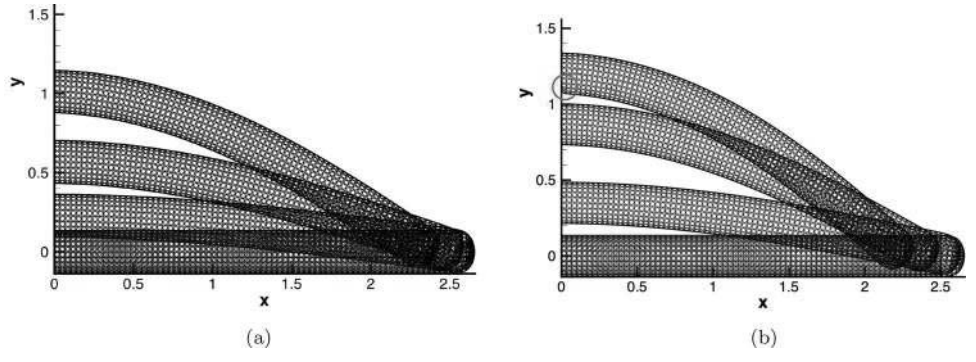

Figure 11. Results of the numerical 3D membrane computations. (a) $Q = 100$ N. (b) $Q = 300$ N.

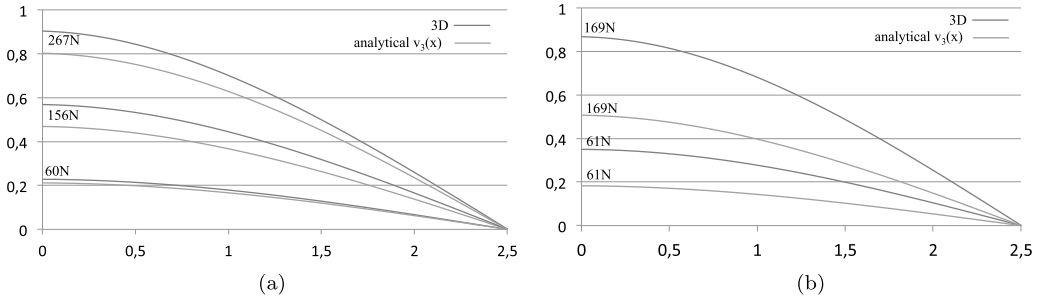

Figure 12. Comparaison between the 3D numerical results ans the theoretical results. (a) $Q = 100$ N. (b) $Q = 300$ N.

Theory for compressed and bent inflatable beams

General solution

To obtain more rigorous results for pressurized and compressed air-beams, it is necessary to restart from the equilibrium equations (4), (5) and (6) and from the boundary conditions (7), (8) and (9). For the general solution, the configuration chosen, the loads applied and the notation used in the following developments are the same as in Figure 6. The initial configuration is the one of the compressed pressurized beam, and the radius R and the length L are obtained with the Equations (18) and (19). This also allows one to calculate the elasticity moduli in the initial configuration from Equations (3).

The normal force is obtained by means of (4) and (7):

$$N(x) = P - Q. \tag{22}$$

Using (5) and (8) leads to

$$\frac{\mathrm{d}v(x)}{\mathrm{d}x} - \theta(x) = -\frac{F_{x2}}{N + kG_{\ell t}S}\,\theta(x) + \frac{F_{y2}}{N + kG_{\ell t}S}. \tag{23}$$

Inserting this result in (6) gives the following differential equation:

$$\frac{\mathrm{d}^2\theta(x)}{\mathrm{d}x^2} - \frac{(P + kG_{\ell t}S)F_{x2}}{(N + kG_{\ell t}S)(E_\ell I + N\frac{I}{S})}\,\theta(x) = -F_{y2}\,\frac{(P + kG_{\ell t}S)}{(N + kG_{\ell t}S)(E_\ell I + N\frac{I}{S})}. \tag{24}$$

As $F_{x2} = -Q$ is negative, the equation can be put in the following form:

$$\frac{\mathrm{d}^2\theta(x)}{\mathrm{d}x^2} + \Omega^2\theta(x) = \Omega^2\frac{F_{y2}}{F_{x2}} \quad \text{where } \Omega^2 = -\frac{P + kG_{\ell t}S}{(N + kG_{\ell t}S)(E_\ell I + N\frac{I}{S})}F_{x2}. \tag{25}$$

The solution of this equation is

$$\theta(x) = A\cos\Omega x + B\sin\Omega x + \frac{F_{y2}}{F_{x2}}, \tag{26}$$

where A and B are constants to be determined with the boundary conditions. Equation (23) can be rewritten:

$$\frac{\mathrm{d}v(x)}{\mathrm{d}x} = \frac{P + kG_{\ell t}S}{N + kG_{\ell t}S}\,\theta(x) + \frac{F_{y2}}{N + kG_{\ell t}S}. \tag{27}$$

The general form of the deflection is deduced by a simple integration which generates an additional

Figure 13. Compressed bended air-beam: notations.

constant C to be determined:

$$v(x) = \frac{P + kG_{\ell t}S}{N + kG_{\ell t}S}\left(\frac{A\sin\Omega x}{\Omega} - \frac{B\cos\Omega x}{\Omega} + \frac{F_{y2}}{F_{x2}}x + C\right) + \frac{F_{y2}}{N + kG_{\ell t}S}x. \tag{28}$$

The three constants A, B and C must be calculated using the boundary conditions.

Solution for the mast and the column

To solve the problem, we use the configuration in Figure 13, for which the clamped end provides two kinematic boundary conditions $v(0) = 0$ and $\theta(0) = 0$. The missing equation to determine the three constants comes from the boundary condition (9) that allows to introduce the torque Γ in the solution.

Imposing $\Gamma = 0$ in the solution found allows to obtain directly the solution for the mast. In this case, the deflection is denoted $v_5(x)$. As for the solution for the column, Γ must be identified using the condition $\theta(L) = 0$ and reinserted into the deflection solution. The expression obtained is $v_6(x)$.

Eventually, the solutions for the cantilever compressed air-beam submitted to a transverse load F and a torque Γ at its free end is

$$\theta(x) = \frac{F}{Q}(-1 + \cos\Omega x + \tan\Omega L\sin\Omega x) + \frac{\Gamma}{(E_\ell I + N\frac{I}{S})}\frac{\sin\Omega x}{\Omega\cos\Omega L} \tag{29}$$

and

$$\begin{aligned} v(x) = {} & \frac{F}{Q}\frac{P + kG_{\ell t}S}{N + kG_{\ell t}S}\left(-x + \frac{\sin\Omega x}{\Omega} + \frac{\tan\Omega L}{\Omega}(1 - \cos\Omega x)\right) \\ & + \Gamma\frac{P + kG_{\ell t}S}{(E_\ell I + N\frac{I}{S})(N + kG_{\ell t}S)}\frac{(1 - \cos\Omega x}{\Omega^2\cos\Omega L} + \frac{Fx}{N + kG_{\ell t}S}. \end{aligned} \tag{30}$$

In the case of the mast, the deflection relation simplifies to

$$v_5(x) = \frac{F}{N + kG_{\ell t}S}\left(\frac{P + kG_{\ell t}S}{Q}\left(-x + \frac{\sin\Omega x}{\Omega} + \frac{\tan\Omega L}{\Omega}(1 - \cos\Omega x)\right) + x\right). \tag{31}$$

The influence of the compressive load Q on the stiffness of the beam is not as visible as in expression (20) for $v_3(x)$, especially since Ω also depends on Q.

In order to determine $v_6(x)$ for the column, the torque Γ is computed from Equation (29) and $\theta(L) = 0$:

$$\Gamma = \left(E_\ell I + N\frac{I}{S}\right)\Omega\left(\frac{\cos\Omega L - 1}{\sin\Omega L}\right)\frac{F}{Q} \tag{32}$$

The solution $v_6(x)$ is given by replacing Γ by its expression (32) in Equation (30). The resulting expression, rather lengthy, is not given here.

Case of small compressive loads

A question then arises, considering the case of the inflatable mast for example, are the solutions $v_3(x)$ Equation (20) and the new solutions $v_5(x)$ consistent?

To answer this question, we shall compare the results given by $v_3(x)$ with the results given by the code SAFE. For small compressive loads, the deflections are found to be correctly calculated. If Q tends to 0, then Ω tends to 0 also. It is then possible to use the Taylor expansions for $\sin \Omega x$ and $\cos \Omega x$: $\sin \Omega x \simeq \Omega x - \Omega^3 x^3/6$ and $\cos \Omega x \simeq 1 - \Omega^2 x^2/2$. As Ω is supposed very small, the approximation $\tan \Omega L \simeq \Omega L$ also holds. Equation (31) then becomes

$$v_7(x) = \frac{F}{N + kG_{\ell t}S}\left(\frac{P + kG_{\ell t}S}{Q}\Omega^2\left(L\frac{x^2}{2} - \frac{x^3}{6} + x\right)\right). \tag{33}$$

Replacing Ω^2 with its expression (25) leads to:

$$v_7(x) = F\left(\frac{(P + kG_{\ell t}S)^2}{(N + kG_{\ell t}S)^2}\frac{1}{(E_\ell I + N\frac{I}{S})}\left(L\frac{x^2}{2} - \frac{x^3}{6}\right) + \frac{x}{N + kG_{\ell t}S)}\right). \tag{34}$$

If Q tends to zero, $N + kG_{\ell t}S$ is equivalent to $P + kG_{\ell t}S$, and finally the Equation (34) becomes:

$$v_7(x) = F\left(\frac{1}{(E_\ell I + N\frac{I}{S})}\left(L\frac{x^2}{2} - \frac{x^3}{6}\right) + \frac{x}{N + kG_{\ell t}S)}\right). \tag{35}$$

Since $N(x) = P - Q$, this gives finally:

$$v_7(x) = F\left(\frac{1}{(E_\ell I + (P - Q)\frac{I}{S})}\left(L\frac{x^2}{2} - \frac{x^3}{6}\right) + \frac{x}{P - Q + kG_{\ell t}S)}\right). \tag{36}$$

$v_7(x)$ is identical to $v_3(x)$ (see (20)). By extension to other configurations, this means that it is possible to account the compression effect of the compressive loads by replacing P with $P–Q$ in the 'usual' solutions of the air-beams in case of low compression.

Buckling load

Before going any further, it is necessary to know the load limits that can be applied to the beam, whether it is a transverse or a compressive load. The compressive load must be lower than the buckling load. This load must be known, and it must be added to the key loads of the beam study: the wrinkling load F_w and the collapse load F_c. The calculation is based on the same equations as for the bending but with $F_{y2} = 0$. One easily obtains

$$\frac{\mathrm{d}^2\theta(x)}{\mathrm{d}x^2} + \Omega^2\theta(x) = 0 \tag{37}$$

whose solution is

$$\theta(x) = A\cos\Omega x + B\sin\Omega x. \tag{38}$$

The two constants A and B can be computed with the boundary conditions. For example, for the mast problem the boundary conditions are $\theta(0) = 0$ and $\mathrm{d}\theta/\mathrm{d}x(L) = 0$. This leads to $cos\Omega L = 0$ and

$$\Omega L = \frac{\pi}{2} + n\pi \quad \text{with } n = 1..\infty \tag{39}$$

Using the expression of Ω^2:

$$\Omega^2 = -\frac{P + kG_{\ell t}S}{(N + kG_{\ell t}S)(E_\ell I + N\frac{I}{S})}F_{x2} = \frac{P + kG_{\ell t}S}{(P - Q + kG_{\ell t}S)(E_\ell I + \frac{(P-Q)I}{S})}Q \tag{40}$$

it then follows that

$$\Omega^2\left[\frac{Q^2 I}{S} - Q\left(E_\ell I + \frac{PI}{S} + \frac{I}{S}(P + kG_{\ell t}S)\right) + (P + kG_{\ell t}S)\left(E_\ell I + \frac{PI}{S}\right)\right] = (P + kG_{\ell t}S)Q. \tag{41}$$

The term $Q^2 I/S$ is often negligible compared to the other terms. The buckling load is then obtained by replacing ΩL with its smallest value: $\Omega L = \pi/2$. The buckling load F_B is then

$$F_B = \frac{E_\ell I + \frac{PI}{S}}{\frac{E_\ell I + \frac{PI}{S}}{P + kG_{\ell t}S} + \frac{4L^2}{\pi^2} + \frac{I}{S}}. \tag{42}$$

Wrinkling load for the compressed air-beam

The second limit load for the study is the transverse load that causes a wrinkle to appear. The distribution of axial stresses is given in Figure 14. The grey distribution represents the result of the pre-tension. The distribution of normal stresses due to the compressive load Q is in red whereas the bending stresses are in black. These distributions can be superimposed to obtain the distribution of normal stresses in the beam represented in blue in Figure 14. The inclined blue line represents the limit of normal stresses when there is no compression. Compression must therefore also be taken into account when determining the wrinkling load. The longitudinal stress is calculated:

$$\Sigma_{xx} = \frac{P - Q}{2\pi R} = \frac{pR}{2} - \frac{Q}{2\pi R}. \tag{43}$$

The relation between the bending moment and the stresses at the upper point of the membrane is $\Sigma_{xx} = FL/\pi R^2$. This leads finally to the wrinkling load:

$$F_W = \frac{p\pi R^3}{2L} - \frac{QR}{2L}. \tag{44}$$

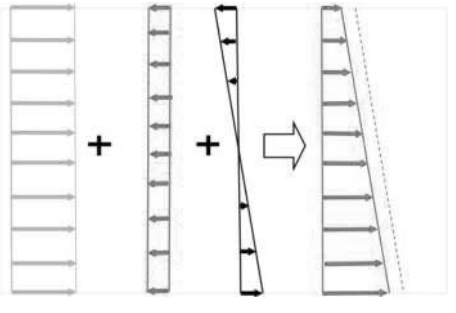

Figure 14. Distribution of the longitudinal stresses in the case of a compresssed bended air-beam.

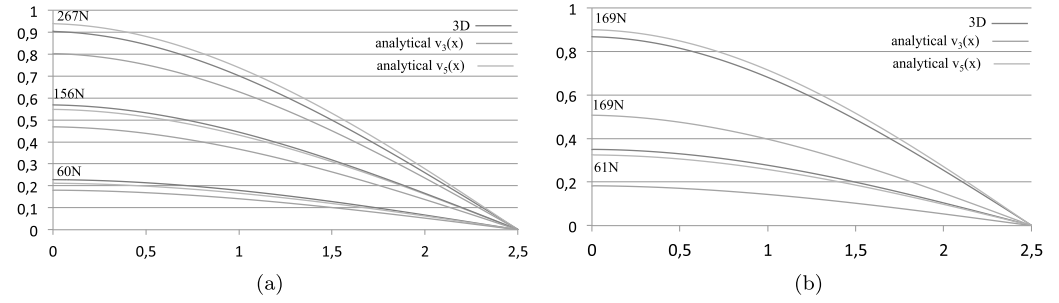

Figure 15. Comparison between the 3D results ans the theoretical results. (a) Q=100 N. (b) Q=300 N.

Comparison with the 3D numerical results

The results for the inflatable mast are compared with the 3*D* code results in order to assess the compressed inflatable beam formula. On both graphs in Figure 15, the results of the 3*D* code are in blue, those of the bending beam $v_3(x)$ in which P is replaced with $P-Q$ in orange, and those of the complete formulation $v_5(x)$ in green. As can be clearly seen, the results of the formulation of the compressed inflatable beam are satisfactory. This is particularly evident on the right graph corresponding to the 300*N* compression load, for which the $v_3(x)$ formula is clearly not satisfactory, while the difference between $v_5(x)$ and the 3*D* code results is very small in comparison.

Analysis of results

Influence of Q in the case of an inflatable mast

Figure 16 shows the influence of the compressive load Q. To study this influence, let us consider the case of the mast, where the inside pressure is constant, the same transverse load is taken equal to $F = 100$ N in all computations, and the compressive load Q is given different values. This shows clearly the effect of the compression. For this example, the radius in the initial position is 0.125 m thus the force P is almost 12 kN which is much larger than the values of Q used for the simulations: 100 N, 200 N, 300 N and 400 N. The ratio between P and Q is less than 4%, but Q has a very significant effect on the deflection. The deflection of the beam without any compression is in red in Figure 16. So, ignoring the effect of the compression can lead to important errors.

Analysis of the results in the case of an inflatable column

Figure 17 gives the results for two configurations: mast and column with the loads already used in the comparison between the analytical results and the 3*D* code results. As predicted, it can be seen that the column is more rigid than the mast. This seems logical, because in the classical beam theory, it can be

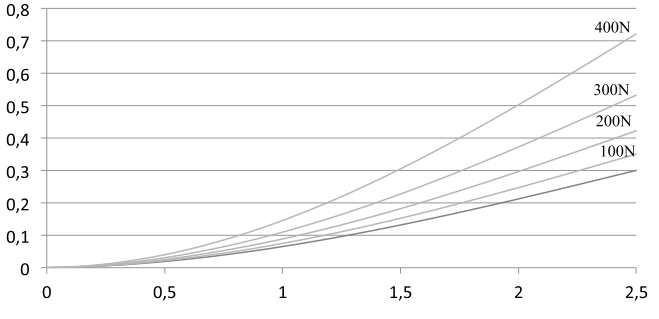

Figure 16. Example of the influence of Q.

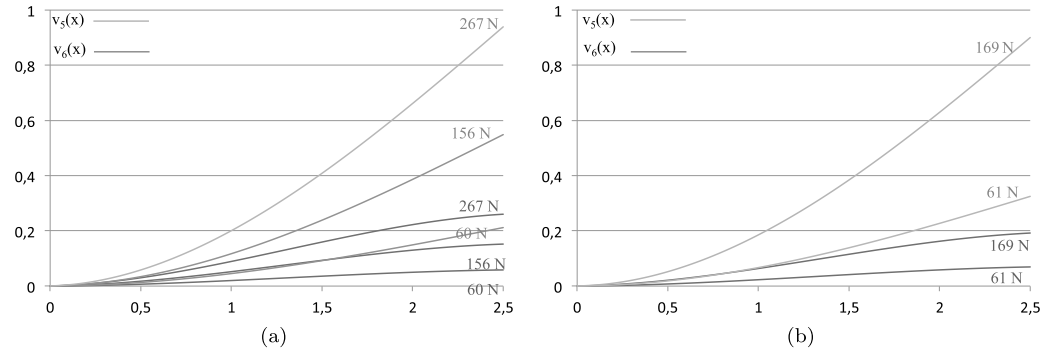

Figure 17. Comparison between the models of the mast and the column for Q= 100 N and Q=300. (a) Q=100 N. (b) Q=300 N.

shown that the ratio is 4 between the two configurations in Figure 8. Even if there is an influence of shear and compression, the main tendency is maintained. Similar results are found for the column and the mast: for the same transverse load, increasing compression means decreasing stiffness.

Conclusion

Air-beams are often subjected to load combinations, mainly bending loads and compression loads. While the theory of bended inflatable beams is well known, the account of the influence of compression on the stiffness of beams has been little studied. In this work, two approaches have been proposed to solve the problem. The first one consists in a direct adaptation of the beam formulas. Its validity domain is very limited because it requires very low compression. A new general formula has been developed and the solutions for the mast and column have been given. A comparison between the new analytical results and the numerical results of the 3D code SAFE shows that the model is very satisfactory.

Disclosure statement

No potential conflict of interest was reported by the author(s).

References

Bridgens, B. N., & Gosling, P. D. (2004). Direct stress-strain representation for coated woven fabrics. *Computers and Structures*, *82*, 1913–1927. https://doi.org/10.1016/j.compstruc.2003.07.005

Bridgens, B. N., Gosling, P. D., Jou, G. -T., & Hsu, X. Y. (2012). Inter-laboratory comparison of biaxial tests for architectural textiles. *Journal of the Textile Institute*, *103*(7), 706–708. https://doi.org/10.1080/00405000.2011.602824

Fichter, W. (1966). *A theory for inflated thin-wall cylindrical beams*. NASA Technical Note, NASA-TND-3466.

Galliot, C., & Luchsinger, R. (2009). A simple model describing the non-linear biaxial tensile behaviour of PVC-coated polyester fabrics for use in finite element analysis. *Composite Structures*, *90*(4), 438–447. https://doi.org/10.1016/j.compstruct.2009.04.016

Le van, A., & Wielgosz, C. (2005). Bending and buckling of inflatable beams: some new theoretical results. *Thin-Walled Structures*, *43*(8), 1166–1187. https://doi.org/10.1016/j.tws.2005.03.005

Motevalli, M., Uhlemann, Y., Stranghöner, N., & Balzani, D. (2019). Geometrically nonlinear simulation of textile membrane structures based on orthotropic hyperelastic energy functions. *Composite Structures*, *223*. https://doi.org/10.1016/j.compstruct.2019.110908

Nguyen, Q.-T, Thomas, J.-C., & Le Van, A. (2013a). An analytical solution for an inflated orthotropic membrane tube with an arbitrarily oriented orthotropy basis. *Engineering Structures*, *56*, 1080–1091. https://doi.org/10.1016/j.engstruct.2013.06.012

Nguyen, Q.-T, Thomas, J.-C., & Le Van, A. (2013b). *An exact solution to calculate the length and radius of an orthotropic inflatable beam – a theoretical application to the determination of the material coefficients*. Proceedings of the tensinet symposium, rethinking lightweight structures, May 8–10, 2013, Istanbul.

Nguyen, Q.-T, Thomas, J.-C., & Le Van, A. (2015). Inflation and bending of an orthotropic inflatable beam. *Thin-Walled Structures*, *88*, 129–144. https://doi.org/10.1016/j.tws.2014.11.015

Quaglini, V., Corazza, C., & Pogi, C. (2008). Experimental characterization of orthotropic technical textiles under uniaxial and biaxial loading. *Composites Part A: Applied Science and Manufacturing*, *39*(8), 1331–1342. https://doi.org/10.1016/j.compositesa.2007.07.008

Tensinet association website. Retrieved from http://www.tensinet.com

Thomas, J.-C., & Bloch, A. (2016). Non linear behaviour of an inflatable beam and limit states. *Procedia Engineering*, *155*, 398–406. https://doi.org/10.1016/j.proeng.2016.08.043

Thomas, J.-C., Le Van, A., Aduriz, X., & Jiang, Z. (2005). Dynamic behaviour of inflatable tubes. *Proceedings of composites in construction 2005, third international conference, July 11, Lyon, France*.

Thomas, J.-C., Schoefs, F., Caprani, C., & Rocher, B. (2018). Reliability of inflatable structures: Challenge and first results. *European Journal of Environmental and Civil Engineering*. Advance online publication. https://doi.org/10.1080/19648189.2018.1474807